Research on Segmentation Algorithms of Retinal Vessel Images

Hao-Ming Song, Yu Liu *, Jie-Sheng Wang, Biao Zhou

Abstract—**Retinal diabetes, hypertension, cardiovascular and cerebrovascular diseases are mostly diagnosed automatically in medicine, and retinal vascular segmentation results have a great impact on them. Because of the tiny blood vessels, pathological changes, central reflection and uneven background brightness in retinal images, the accuracy of blood vessel segmentation is low. Because the illumination of blood vessel pixels and background pixels in fundus image is uneven and the contrast is low. In this paper, data standardization, mathematical morphology, adaptive histogram equalization, gray conversion and gamma correction are used to carry out preparatory processing on images of retinal blood vessels, which can not only detect the characteristics of small blood vessels more accurately, but also improve the performance of network segmentation. Then, the retinal vessel images are segmented based on six segmentation algorithms: maximum variance between classes, region growing, Sobel operator, iterative threshold method, quad-tree image segmentation and mathematical morphology algorithm. Simulation experiments are carried out to verify the effectiveness of the segmentation algorithms for typical retinal vessel images in Drive library.**

Index Terms—**retinal vessel image, segmentation algorithm, performance comparison**

I. Introduction

FROM can be seen in the retinal fundus images, such as macular degeneration, glaucoma, diabetic retinopathy, these phenomenon, is due to the vascular diameter, curvature and Angle change, when these diseases occur and didn't get timely treatment, will lead to deterioration that blindness, and even more serious consequences. The segmentation results of retinal blood vessels have guiding significance for the automatic diagnosis of retinal diabetes, hypertension, cardiovascular and cerebrovascular diseases. Because of tiny blood vessels, pathological changes, central reflection and uneven background brightness in retinal images, the accuracy of blood vessel segmentation is lower [1]. Therefore, effective segmentation of retinal fundus images not only contributes to the early diagnosis of vascular abnormalities, but also has a great impact on the defense and treatment of some ophthalmic diseases. The meaning of image segmentation is to segment the image into a number of specific and unique regions, which all have similar properties, such as gray scale, color, texture, brightness, contrast and so on, and then select the part of interest and put it into practice. Region based segmentation, edge based segmentation, level set based segmentation and other segmentation methods are commonly used in medical segmentation [2]. These segmentation methods, including classifier and cluster, threshold method, random field method, region growth method and split-merge method, are all based on region. Among them, because the pixel gray value at the edge of the region changes dramatically, the edge segmentation method mainly relies on the edges between different regions to solve the problem of image segmentation ,surface fitting method, boundary curve fitting method, serial boundary search method and deformation model-based method [3-4].

In recent years, the segmentation algorithm of retinal vessels has been studied by many researchers. Fraz et al. summarized research methods for vascular segmentation, which mainly divided segmentation algorithms into unsupervised methods and supervised methods [5]. Among these methods, the characteristic of unsupervised algorithm is that it does not need to label its label data manually. Its most commonly used methods include vascular tracking, active contour model, matched filtering and graph-based model, etc. Chaudhuri et al. used the matched filtering method to find that the cross-section gray profile and similarity of blood vessels follow Gaussian curve form, but the detection accuracy of this technique is very low [6]. Matched filtering has limitations. Its defects are that it cannot accurately segment low-contrast areas and vessels with central reflection, which is caused by pathological factors. [7-9]. Using local information to segment the blood vessels between two points is a vascular tracing method, and the key to detect blood vessels is the seed point . The width of the blood vessel is accurately calculated by determining the center of the longitudinal section of the blood vessel by using the gray intensity and the curvature. However, a defect of this method is that it cannot detect vessels without seed points, so the accuracy of vessel segmentation is not high [10-12]. Chowdhury et al. proposed a method based on morphological processing to detect blood vessels and background regions, and then classified pixels by Gaussian mixture model [13]. Zana and other scholars proposed a method of vascular detection based on mathematical morphology and curvature assessment [14].

Manuscript received August 16, 2021; revised November 5, 2021. This work was supported by the Basic Scientific Research Project of Institution of Higher Learning of Liaoning Province (Grant No. 2019LNQN10), and the Project by Liaoning Provincial Natural Science Foundation of China (Grant No. 20180550700).

Hao-Ming Song is a postgraduate student of School of Electronic and Information Engineering, University of Science and Technology Liaoning Anshan, 114051, P. R. China. (e-mail: 823234816@qq.com).

Yu Liu is a lecturer of School of Electronic and Information Engineering, University of Science and Technology Liaoning, Anshan, 114051, P. R. China. (Corresponding author, phone: 86-0412-2538355; fax: 86-0412-2538244; lnasacl@126.com).

Jie-Sheng Wang is a professor of School of Electronic and Information Engineering, University of Science and Technology Liaoning, Anshan, 114051, P. R. China. (e-mail: wang_jiesheng@126.com).

Biao Zhou is an undergraduate student of School of Electronic and Information Engineering, University of Science and Technology Liaoning, Anshan, 114051, P. R. China. (e-mail: zhoubiao@youopto.com).

The supervised learning method needs blood vessel and non-blood vessel sample data manually marked by ophthalmologists, and realizes blood vessel segmentation by classifying blood vessel pixels and background pixels. Supervised learning into feature extraction and classification of two periods, which is divided into artificial feature extraction of feature extraction and mechanical automatic extraction ability of learning, and it have four kinds of classification methods, K nearest neighbor (KNN), Gaussian mixture model (GMM), support vector machine (SVM) and artificial neural network (ANN) [15-17]. Scholars represented by Hassan proposed a fusion of morphological science and another K-means clustering method to segment retinal blood vessels Hassan et al [18]. Ricci et al. proposed a segmentation method based on the prior operation and support vector machine segmentation of retinal vessels [19]. Based on the maximum variance between classes method, region growing method, Sobel operator, iterative threshold method and quad-tree image segmentation and mathematical morphology algorithm are adopted to segment the retinal vessel images.

II. Retinal Vessel Image Segmentation and Database

A. Retinal Vessel Image Segmentation

The amount of information obtained by eyes is as high as 90%. The early stage of some diseases can be realized by observing, reasoning and analyzing the morphological changes of eyes. Seen from cross section, the shape of human eye is similar to a sphere, including eye wall, contents, nerves, blood vessels and other tissues. The inner membrane of the eye is the retina, which is located in the innermost layer of the eye and is distributed with a large number of photoreceptor cells. It is the most sensitive area of nerve transmission in visual formation. Retina is the sensory membrane of eyes, which is responsible for vision, mainly including optic disc, macula, blood vessels and other anatomical parts. The fundus optic disc is light yellow, and the retina enters and exits the eye through fibers and retinal blood vessels. Macular area is the optical center of human eyes, located directly below the horizontal line of optic disc. Retina has the best resolution in macular area. The macular area has no blood vessels and is rich in lutein. Under ophthalmoscope, the color is slightly dark, which has certain influence on retinal vessel segmentation. Retinal image acquisition is a very complex optical imaging system, which is called fundus camera. In panchromatic mode, the retina is illuminated with white light to obtain a panchromatic (RGB) image. When there is no red mode, the contrast of retinal blood vessels and other structures is higher, and the red components are filtered out. In fluorescein angiography mode, fluorescein sodium is injected into blood vessels, the retinal blood vessels are obviously enhanced under ultraviolet light, and then retinal angiographic images are extracted. It can be seen from the retinal images that the retinal blood vessel consists of two parts. The arteries and veins are very thin, and the branches of blood vessels are clearly visible. The width element of retinal blood vessels varies greatly, which is closely related to the vascular structure and image resolution. Other structures in the image mainly include retinal boundary, flocculent lesions, macular and eye exudates, etc. At the same time, the direction and gray value of blood vessels show linear changes locally, and change slowly with the increase of blood vessel length so as to form a binary tree structure. Meanwhile, in the whole retinal vascular network, the shapes, sizes and gray values of blood vessels are diversified, and the gray values of some background pixels are similar to those of blood vessels, which also increases the difficulty of blood vessel segmentation. The effective segmentation of retinal fundus images not only benefits the early diagnosis of vascular abnormalities but also has a qualitative leap in the prevention and treatment of other eye diseases.

B. Retinal Vessel Image Database

The images of retinal image database can be used as experimental data to test and evaluate the segmentation algorithms. Drive database is an open database with 40 fundus color pictures and retinal vessel images manually segmented by two experts. In 40 images, 7 lesions included exudate, epithelial cytochrome changes and hemorrhage. Partial results of manual segmentation of normal and pathological color fundus images in Drive database are shown in Fig. 1. These 40 images are divided into testing set and training set, each set contains 20 images. For manual segmentation results, the first expert mark is 12.7% and the second expert mark is 12.3%. Therefore, this paper chooses the first expert's manual segmentation result as the segmentation standard of retinal blood vessel images.

III. Image Segmentation Algorithms

A. Maximum Variance between Classes

The method of maximum variance between classes, also known as OTSU, is derived from the least square method. In its calculation logic, all images are divided into two groups, and the threshold value is set as the gray value of a fixed value. After variance calculation, the threshold value is used as the dividing line to realize image segmentation:

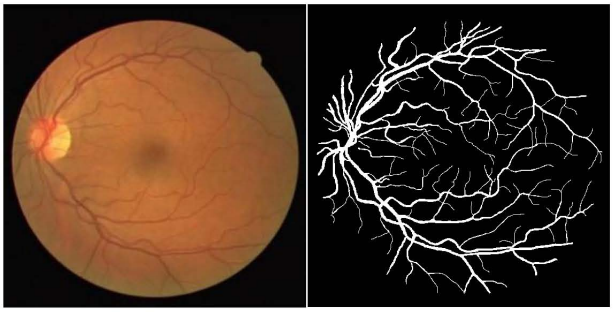

(a) Normal color retinal image 1 and manual segmentation results

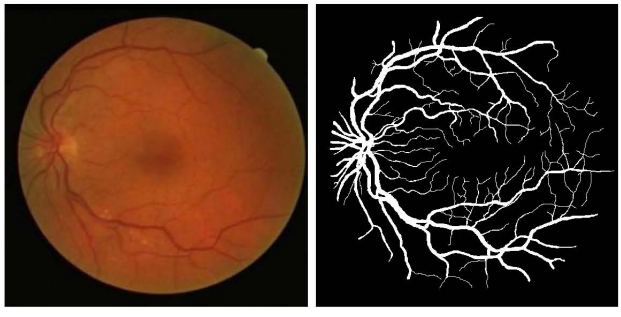

(b) Normal color retina image 2 and manual segmentation results

Fig. 1 Retinal vessel image and segmentation result in DRIVE database.

$$N = \sum_{i=1}^{m} n_i \quad (1)$$

The probability of gray value is calculated by:

$$P = \frac{n_i}{N} \quad (2)$$

Then divide them into two groups by k value: $C_0 = [1 \cdots K]$ and $C_1 = [K+1 \cdots m]$, then the probability of C_0 production is calculated by:

$$\omega_0 = \frac{\sum_{i=1}^{k} n_i}{N} = \sum_{i=1}^{k} P_i \quad (3)$$

The production probability of Group C_1 is defined as:

$$\omega_1 = \frac{\sum_{i=k+1}^{m} n_i}{N} = \sum_{i=k+1}^{m} P_i = 1 - \omega_0 \quad (4)$$

The average gray value of the group C_0 is defined as:

$$u_0 = \frac{\sum_{i=1}^{m} n_i * i}{\sum_{i=1}^{m} n_i} = \frac{\sum_{i=1}^{m} P_i * i}{\omega_0} \quad (5)$$

The average gray value of the group C_1 is defined as:

$$u_1 = \frac{\sum_{i=k+1}^{m} n_i * i}{\sum_{i=k+1}^{m} n_i} = \frac{\sum_{i=k+1}^{m} P_i * i}{\omega_1} \quad (6)$$

The overall average gray value is defined as:

$$u = \sum_{i=1}^{m} P_i * i \quad (7)$$

where, the average value of gray scale when the threshold value is k can be calculated by:

$$u(k) = \sum_{i=1}^{k} p_i * i \quad (8)$$

The average gray value of sampling is $\mu = \omega_0 u_0 + \omega_1 u_0$, and the variance formula between the two groups is described as:

$$d(k) = \omega_0 (u_0 + u)^2 + \omega_1 (u - u_1)^2 \quad (9)$$

Bring the overall average gray value into the variance formula between two groups so as to obtain:

$$d(k) = \omega_0 \omega_1 (u_1 - u_2)^2 \quad (10)$$

In this way, the value of k is changed from 1 to m, and the obtained k^* is satisfied with $d(k^*) = \max(d(k))$. Then segment the image with the threshold k^* so that the best segmentation results can be obtained.

B. Regional Growth Method

Region growing method is based on general heuristic method and original uniformity standard, which can reduce the minimum number of regions that can't be combined with adjacent regions in segmented images and obtain image segmentation information. Regional adjacency graph (RAG) represents the regional adjacency. The region is represented by the node set in rag, $n = \{N_1, N_2, ..., N_M\}$ where the node N_i represents the region in the scene, and the region information RI is stored in the node data structure N_i. The edge between N_i and $N_j$represents the connection between RI and the region. Keep the pixels in adjacent areas where RI and PI are adjacent. The adjacency can be 4-connection or 8-connection. Fig. 2(a) shows the scene adjacency graph with six different regions, and Fig. 2(b) shows the adjacency matrix of multi-region scenes.

C. Sobel Operator

Sobel operator is a discrete difference operator, and it is widely used, such as approximate calculation of function gray value and image brightness calculation. Fig. 3 shows Sobel convolution factor. Eq. (11) is the expression of Sobel convolution factor, and its matrix is composed of horizontal and vertical data. Assuming that A is the original image, the following formula is the gray value of the image detected from the horizontal edge and vertical edge respectively.

$$G_x = \begin{bmatrix} -1 & 0 & +1 \\ -2 & 0 & +2 \\ -1 & 0 & +1 \end{bmatrix} * A \text{ and } G_y = \begin{bmatrix} +1 & +2 & +1 \\ 0 & 0 & 0 \\ -1 & -2 & -1 \end{bmatrix} * A \quad (11)$$

When $f(x, y)$ represents the gray value of an image point (a, b), the horizontal and vertical gray value of each pixel of the image are combined by Eq. (12) to calculate the gray level of the point.

$$G = \sqrt{G_x^2 + G_y^2} \quad (12)$$

In order to simplify the calculation and improve the calculation efficiency, the following square root-free approximation is adopted.

$$G = |G_x| + |G_y| \quad (13)$$

If the gradient G is higher than a certain threshold, then this point (x, y) is the edge point. Then, the gradient direction can be calculated by Eq. (14).

If the gradient G is higher than a certain threshold, then this point (x, y) is the edge point. Eq. (14) can then be used to calculate the gradient direction.

$$\theta = arctant\left(\frac{G_y}{G_x}\right) \quad (14)$$

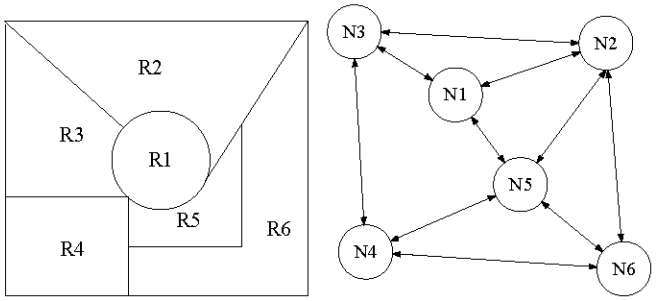

(a) Scenes with six distinct areas (b) Adjacent scenes

Fig. 2 Schematic flow of region growth method.

-1	0	+1
-2	0	+2
-1	0	+3

(a) Sobel convolution factor G_x

+1	+2	+1
0	0	0
-1	-2	-1

(b) Sobel convolution factor G_y

Fig. 3 Sobel convolution factor.

Sobel operator can provide more accurate information about the direction of the edge, that is, it can smooth out the noise, but it has the disadvantage of low accuracy.

D. Iterative Threshold Method

The main idea of iterative threshold image segmentation is described as follows. The average of A and B parts after image segmentation remained the basic stability. That is, through iteration, the final convergent value of $[\text{mean}(A) + \text{mean}(B)]/2$ is taken as the segmentation threshold. The iterative threshold image segmentation process is shown in Fig. 4, and the specific flowchart is described as follows.

Step 1: Select an initial threshold value T.

Step 2: The threshold value T is used to divide the given images into two groups, which are recorded as $R1$ and $R2$ respectively.

Step 3: Select a new threshold value T, $T = (\mu 1 + \mu 2)/2$.

Step 4: Repeat Step 2 to 4 until the difference between T is less than the present value.

E. Quad-tree Image Segmentation Algorithm

Firstly, the image or raster map is encoded and divided into four first-level blocks in the order of upper left, upper right, lower left and lower right. Then check block by block, and attribute (or gray) all grids. If they are the same, the region is no longer divided; otherwise, the sub-block is divided into four small blocks again. Segmentation is performed recursively, until the attribute or gray level of each sub-block is equal. According to the similarity rule, many image segmentation algorithms, such as K-means clustering algorithm, are used because the highly similar pixels in the image are grouped together to form a region. Quad-tree image segmentation algorithm is an image segmentation algorithm based on minimum spanning tree, and its coding schematic is shown in Fig. 5.

Each pixel in the image is regarded as a vertex of the graph, and then the similarity of four or eight neighborhoods of each pixel is calculated according to the similarity rule. These similarities are taken as the weights of the corresponding edges. Then, pixels are merged according to the minimum spanning tree algorithm to obtain multiple minimum spanning trees. At this time, the image is divided into a plurality of regions. The simplest idea of similarity measurement is to measure similarity directly by using Euclidean distance between pixels.

$$S = \sqrt{(r_i - r_j)^2 + (g_i - g_j)^2 + (b_i - b_j)^2} \tag{15}$$

where, S represents the dissimilarity, and s, g and b represent the values of R, G and B components of the color image respectively. The whole algorithm can be expressed as: ∃ Segmentation S, which divides the image I into several regions $\{ C_1C_2\cdots C_n \}$, and define the internal difference function $Int(C)$ of the region.

$$Int(C) = max_{e\in MST(C,\tau)}\omega(e) \tag{16}$$

The internal difference value is equal to the maximum value of the minimum spanning tree edge. Define the inter-regional difference function $Dif(C_1, C_2)$:

$$Dif(C_1, C_2) = min_{v_i\in C_1, v_j\in C_2,(v_i,v_j)\in E}\omega\left((v_i, v_j)\right) \tag{17}$$

Eq. (17) shows that the difference between two regions is the minimum weight of the edge connected by the points on the boundary of two regions. Define the minimum intra-area difference function $MInt(C_1, C_2)$:

$$Mint(C_1, C_2) = min\left(Int(C_1) + \tau(C_1), Int(C_2) + \tau(C_2)\right) \tag{18}$$

where:

$$\tau(C) = \frac{k}{|C|} \tag{19}$$

Define consolidation policy:

$$D(C_1, C_2) = \begin{cases}\text{True if } Dif(C_1, C_2) > Mint(C_1, C_2)\\ \text{False otherwise}\end{cases} \tag{20}$$

When the difference between regions is greater than the minimum difference within the region, these two regions cannot be merged, otherwise they can be merged. When the adjustable parameter K is large, it means that there are great differences in the minimum area of these two areas, and it is difficult to merge, so the algorithm tends to divide the image into many small areas. When the smaller K is selected, the algorithm will divide the image into several large areas.

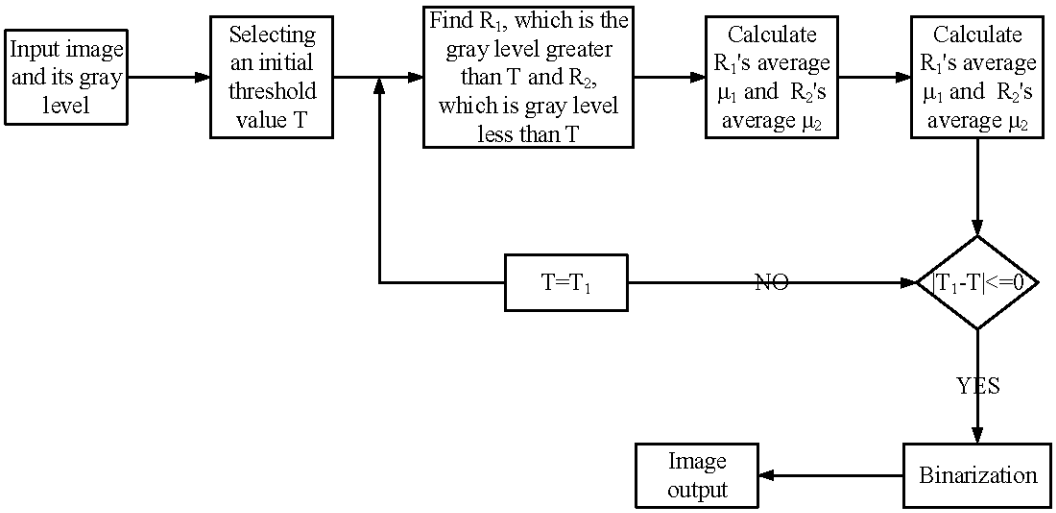

Fig. 4 Flowchart of iterative threshold algorithm.

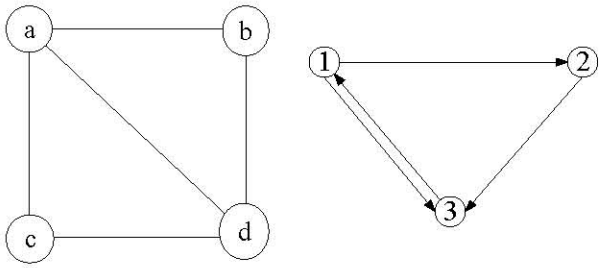

(a) Undirected graph *G*1 (b) Directed graph *G*2

Fig.5 Schematic diagram of quad-tree image coding.

F. Mathematical Morphology Algorithm

Mathematical morphology can be divided into binary morphology and gray morphology. Gray-scale morphology is the deformation of binary morphology. Corrosion and swelling are two basic operations of mathematical morphology. The combination of the two forms open operation and closed operation. Open operation is corrosion and re-expansion, closed operation is expansion and re-corrosion.

1) Binary Morphology

The essence of reducing the scope of target area caused by corrosion is to narrow the image boundary, which can eliminate small objects and meaningless objects. Eq. It can be observed from formula (21) that structure B corrodes structure A. It is worth noting that the origin definition is required in structure B. If the origin in B moves to the image a(x,y) pixel and B is at (x,y) position, then it is fully contained by the overlapping region of A. The binary morphology is shown in Fig. 7. B slides on A in sequence. When the coverage area is $[1, 1;\ 1, 1]$ or $[1, 0;\ 1, 1]$ is A, the position corresponding to the output image is 1.

$$A - B = \{x, y|(B)_{xy} \in A\} \tag{21}$$

2) Expansion

Simply put it and the target range of the region is "expanded" by expansion, and then the target object will merge with the background points that touch the target area, thus causing the edge of the target to extend outward. This behavior results in the function of filling holes in the target area, which can eliminate small particle noise. Formula (22) below represents the expansion of structure B to structure A, smoothing the origin of structure element B to the target position of image pixel (x, y). If the value of the output image (x, y) is 1, the intersection of B and A at the image (x, y). is not empty, otherwise, the output value is 0. Fig. 7 shows the operation of binary graph expansion.

$$A + B = \{x, y|(B)_{xy} \cap A \neq \emptyset\} \tag{22}$$

3) Corrosion of Gray Morphology

For gray-scale morphology, the area of image a covered by structural element b is set as P. Erosion is a vortex-like action. P minus the structural element b forms a small rectangle, and the minimum value is divided by the corresponding origin position. Input images and structural elements (gray is the structural origin) are shown in Fig. 8. The process of gray morphology etching is shown in Fig. 9. The area covered by b is a subtraction matrix firstly, and then min (minimum value) is calculated as the value of the corresponding position of the original point in its difference matrix.

$$\begin{bmatrix}0 & 0 & 0\\ 0 & 4 & 3\\ 0 & 3 & 5\end{bmatrix} - \begin{bmatrix}0 & 1 & 0\\ 1 & 2 & 1\\ 0 & 1 & 0\end{bmatrix} = \begin{bmatrix}0 & -1 & 0\\ -1 & 2 & 2\\ 0 & 2 & 5\end{bmatrix} \tag{23}$$

4) Expansion of Gray Morphology

The expansion operation of gray morphology is similar to corrosion. Expansion is a convolution operation in gray morphology. Add B to p, and then assign the maximum value of the region to the position corresponding to the origin of structural element B . The expansion process of gray morphology is shown in Fig. 10. Sum up the matrix, the maximum value is 6, and assign 6 to the position corresponding to the origin structure of the element.

$$\begin{bmatrix}0 & 0 & 0\\ 0 & 4 & 3\\ 0 & 3 & 5\end{bmatrix} - \begin{bmatrix}0 & 1 & 0\\ 1 & 2 & 1\\ 0 & 1 & 0\end{bmatrix} = \begin{bmatrix}0 & 1 & 0\\ 1 & 6 & 4\\ 0 & 4 & 5\end{bmatrix} \tag{24}$$

The corroded pixels are much smaller than any of the original image pixels, so they are also better for removing peak noise. Conversely, the expansion of the gray value makes all pixels larger than the original pixel, so it is better for filtering valley noise. There are two basic superposition operations: open operation and closed operation, in which corrosion is followed by expansion is open operation, and the opposite is closed operation.

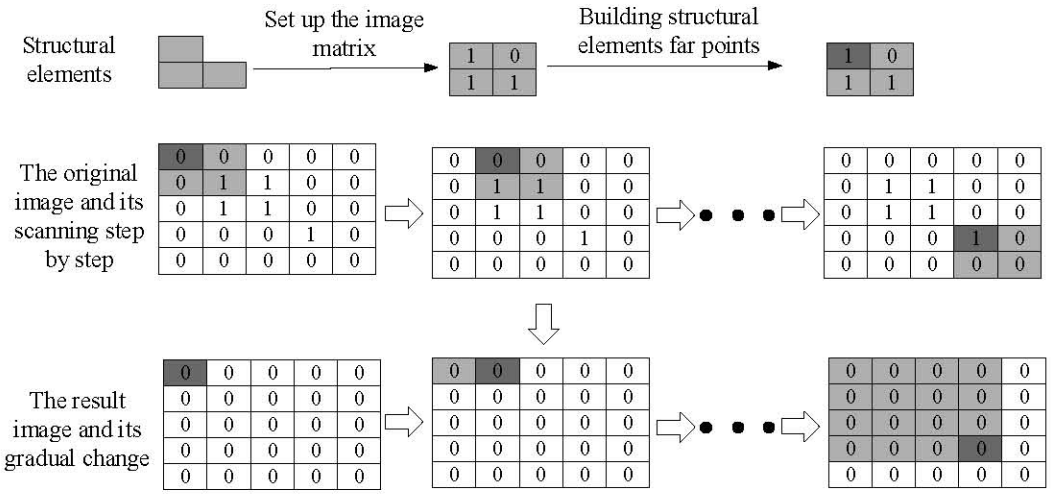

Fig. 6 Demonstration diagram of binary morphology.

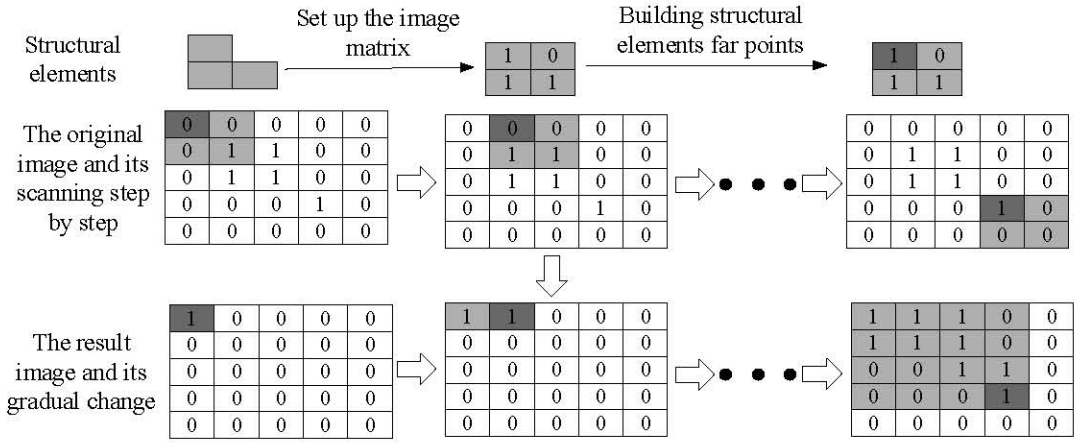

Fig. 7 Schematic diagram of binary image expansion operation.

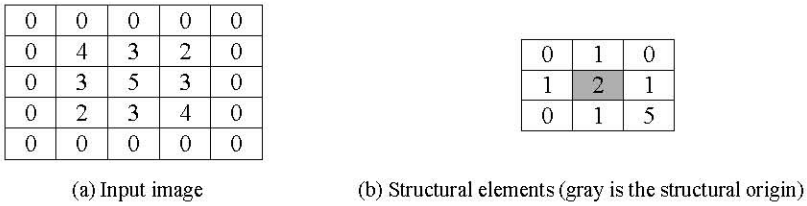

(a) Input image (b) Structural elements (gray is the structural origin)

Fig. 8 Gray scale morphology.

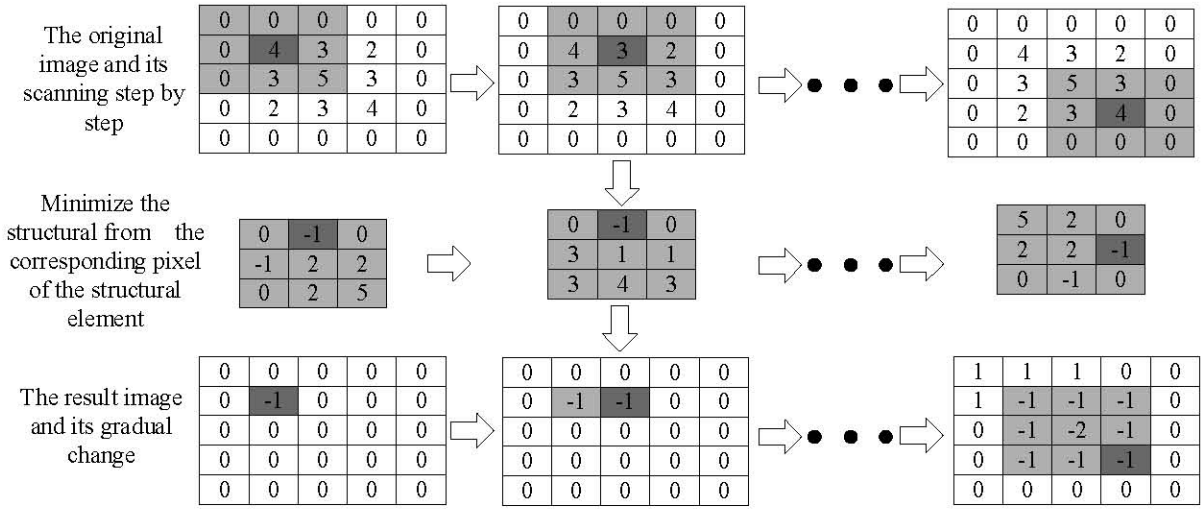

Fig. 9 Schematic diagram of gray image corrosion operation.

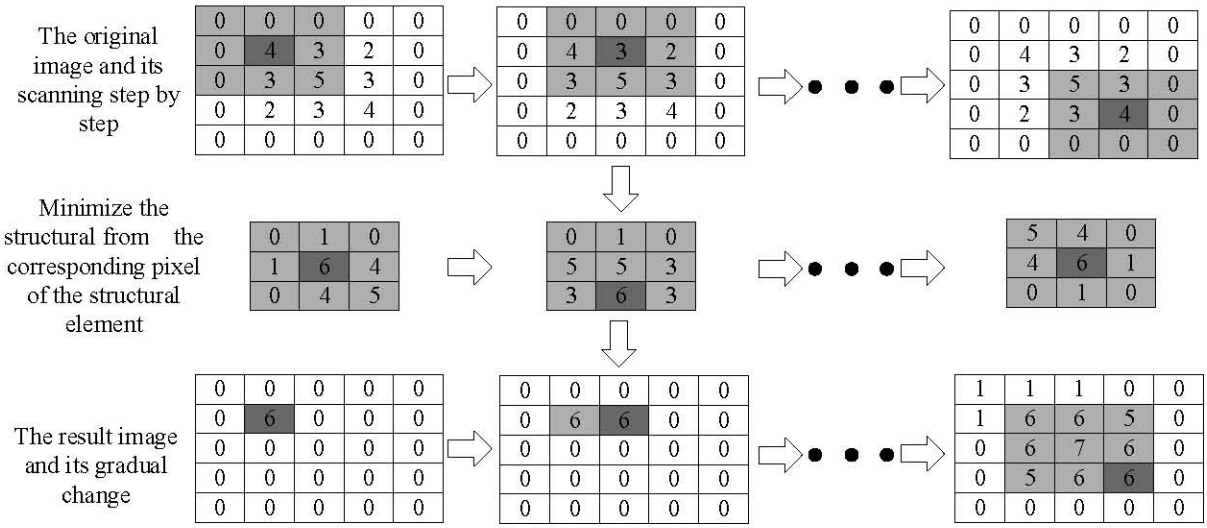

Fig. 10 Schematic diagram of gray scale expansion operation.

IV. Retinal Vessel Image Segmentation Experiments and Result Analysis

A. Performance Evaluation Index of Image Segmentation

The purpose of retinal image blood vessel segmentation is to obtain the classification results of all pixels in the image, and to determine whether they are vascular or background pixels. In order to evaluate the performance of retinal blood vessel segmentation using pixel segmentation method in this paper, the following indicators are selected to evaluate the performance, specificity, accuracy, and area under curve ROC. Among them, sensitivity is the correct ratio detected between vascular pixels and total vascular pixels; the correct ratio of specific non-vascular pixels to total non-vascular pixels; the ratio of correct vascular pixels and non-vascular pixels to total pixels detected is accuracy, which is defined as follows:

$$\mathrm{Se} = \frac{TP}{TP+FN} \tag{25}$$

$$\mathrm{Sp} = \frac{TN}{FP+TN} \tag{26}$$

$$\mathrm{Acc} = \frac{TP+TN}{TP+FN+TN+FP} \tag{27}$$

Among them, the vessel pixel as the correct classification is true positive (TP); correctly classified non-vascular pixels are called true negatives (TN); Misclassified vascular pixels are called false positives (FP); Non-vascular pixels that are misclassified are called false negatives (FN).

Here, the operating characteristic curve becomes the key curve used to measure the dichotomous segmentation synthetic curve. The horizontal and vertical coordinates of ROC curve are false positive rate (FPR) and true positive rate (TPR) respectively. The closer it gets to the top-left curve, the more accurate it gets. Therefore, false positive rate and true positive rate can be defined as:

$$TPR = \frac{TP}{TP+FN} \tag{28}$$

$$FPR = \frac{TP}{FP+TN} \tag{29}$$

B. Preprocessing of Retinal Vessel Images

Because the illumination of blood vessel pixels and background pixels in fundus image is uneven and the contrast is low, in order to better detect the characteristics of small blood vessels and improve the segmentation performance, the fundus image needs to be preprocessed.

(1) Gray scale conversion. According to the gray conversion method defined in Eq. (30), the data values of red, green and blue channels of color fundus image are converted, where Gray represents gray value, R represents red channel, G represents green channel and B represents blue channel.

$$Gray = R * 0.299 + G * 0.587 + B * 0.114 \tag{30}$$

(2) Data standardization. Calculate the mean and standard deviation of gray fundus image, and make the processed data conform to the normal distribution. Standardization operation can be defined as:

$$x_s = \frac{x_g - \mu}{\sigma} \tag{31}$$

where, x_s is the gray image sample data, μ is the data mean, σ is the standard deviation of data, x_g is the normalized image data.

(3) The adaptive histogram equalization algorithm with limited contrast can redistribute the brightness, and changing the image contrast can obviously enhance the local contrast and image details. After standardizing the data of image contrast enhancement, the noise in the local area of the image can be well suppressed, and contrast enhancement can effectively enhance the distinction

(4) Gamma correction. Gamma correction is a nonlinear operation, which can enhance the dark blood vessel area in the fundus retinal image without affecting the area with strong brightness. Its definition can be described as follows.

$$f(I) = I^{\gamma} \tag{32}$$

where, I is the input image data, γ is the value of setting adjustment, and $f(I)$ is the output image data.

(5) Data standardization can adjust the distribution range of image pixel values (0-1). After normalizing the data, it is not only convenient for future data processing, avoiding excessive training gradient, but also speeding up the convergence speed of the model. Data normalization can be defined as:

$$x_{out} = \frac{x_{in} - min}{man - min} \tag{33}$$

where, x_{in} is the pixel value of input image, the maximum and minimum values in the data are represented by Max and min respectively, while x_{out} represents the pixel value of the normalized data.

C. Selection of Retinal Vessel Images and Segmentation Methods

In order to analyze the performance of retinal vessel image segmentation algorithm, this paper selects five typical image segmentation algorithms (maximum between-class variance method, region growing method, Sobel operator, iterative threshold method and quadtree method) for carrying out the simulation experiments. The emphasis is to study the influence of noise, tiny blood vessels and broken blood vessels in the segmentation on the retinal vessel images. Five typical images in Drive retinal blood vessel image library are selected for segmentation experiments. Fig. 11 (a)-(e) are retinal vessel images without lesions and abnormalities, and Fig. 12 (a)-(e) are standard segmentation images of retinal blood vessel images without lesions and abnormalities.

(a) Original figure 1 (b) Original figure 2

(c) Original figure 3 (d) Original figure 4

(e) Original figure 5

Fig. 11 Images of retinal vessels without lesions and abnormalities.

(a) Standard figure 1 (b) Standard figure 2

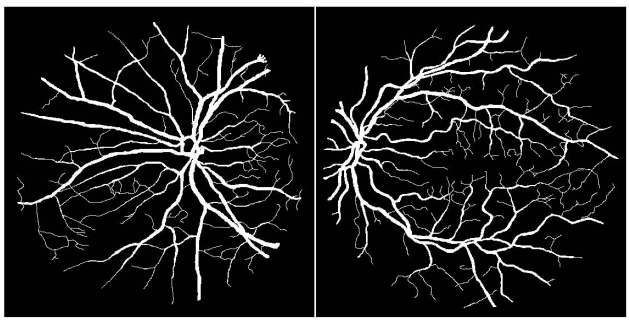

(c) Standard figure 3 (d) Standard Figure 4

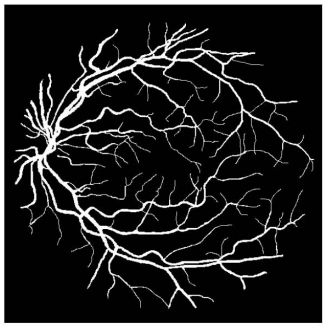

(e) Standard Figure 5

Fig. 12 Standard segmentation of retinal vessel images without lesion and abnormality.

D. Retinal Vessel Image Preprocessing Result

Among them by gamma correction, adaptive gray-scale transformation, histogram equalization, mathematical morphology, data standardization of these methods for the pretreatment of the retinal blood vessel image has carried on the comprehensive processing, such not only takes into consideration the blood vessels of fundus image pixel and background pixels of non-uniform illumination and low contrast, and can better observe monitoring the characteristics of the small blood vessels, Moreover, the performance of network segmentation is greatly improved. When preprocessing images of retinal vessels without lesions or abnormalities in Fig. 11(a)-(e), the results shown in Fig. 13 will be generated. It can be seen that the image segmentation effect can be significantly improved in this way.

E. Retinal Vessel Image Segmentation Results

Five image segmentation algorithms including maximum variance between classes, region growing method, Sobel operator, iterative threshold method and quad-tree method are used to carry out simulation experiments. The segmentation results are compared with the standard segmentation images of retinal vessel images without lesions and abnormalities shown in Fig. 12(a)-(e).

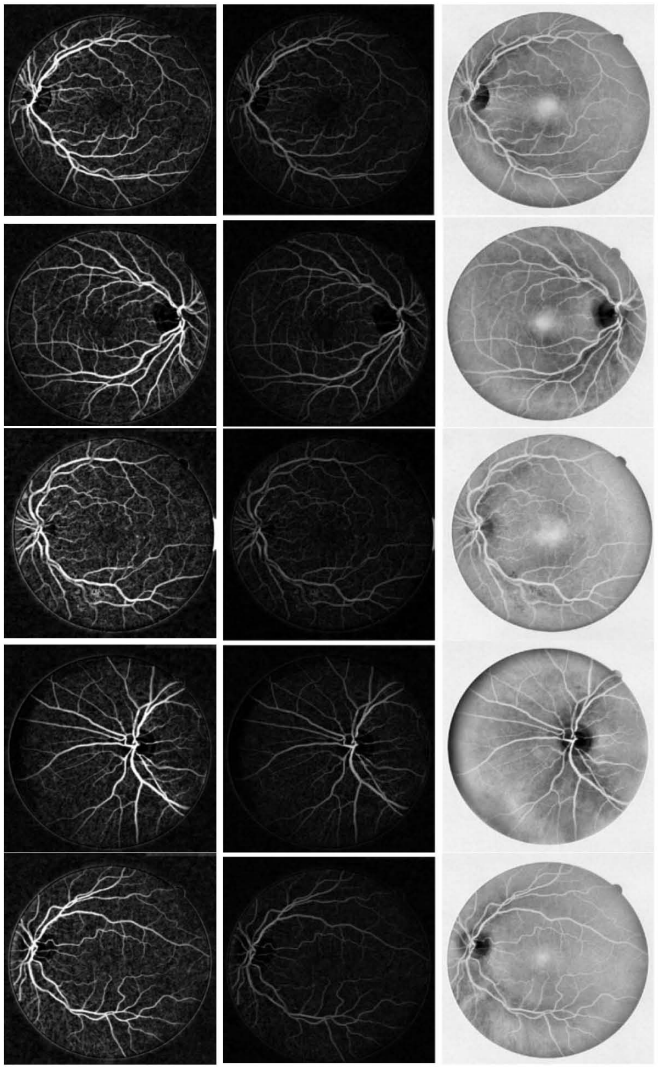

(a) Morphology (b) Histogram equalization (c) Median denoising

Fig. 13 Preprocessing results of retinal vessel images.

The results are shown in Fig. 14-18. The good segmentation effect of small vessels can be reflected by the iterative threshold and region growth method, which does not produce a large error on the standard map, which is intuitively seen from the results of retinal vessel segmentation experiment. Five image segmentation algorithms, including maximum variance between classes, region growing method, Sobel operator, iterative threshold method and quad-tree method, were used to segment the retinal vessel images without lesion and abnormality shown in Fig. 11(a)-(e). The segmentation results are compared with the standard segmentation images of retinal vessel images without lesion and abnormality shown in Fig. 14-18 (a)-(e). The image segmentation performance evaluation results are listed in Tables 1-5. From the above segmentation results on retinal vessel images, the iterative threshold method and region growing method have better segmentation effect on small blood vessels in retina, and there is no big error with standard images. The algorithm of maximum variance between classes can segment the main body and branches of blood vessels well, but there are still breakpoints for the ends. The region growing method is somewhat similar to Sobel operator, which greatly improves the overall segmentation, further divides the vessel diameter and makes the blood vessel display clearer.

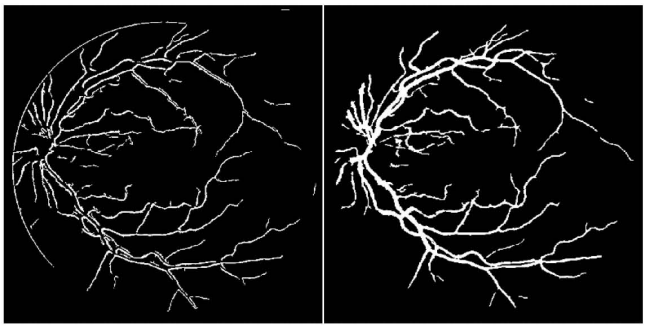

(a) Sobel operator (b) Iterative threshold method

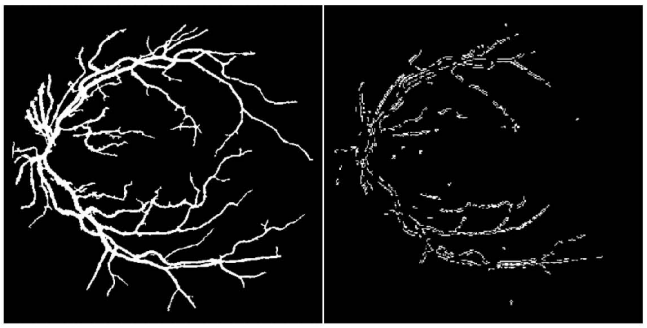

(c) Region growing method (d) Quadtree image segmentation algorithm

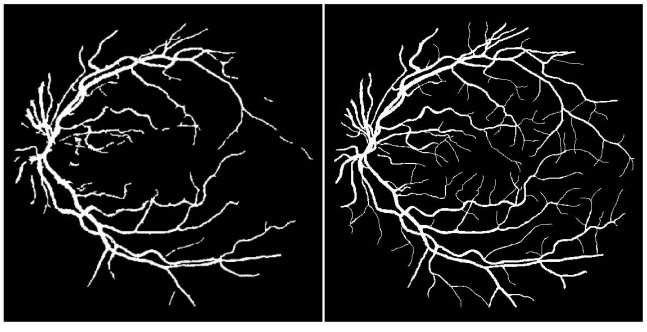

(e) Maximum variance between classes (f) Standard segmentation image

Fig. 14 Retinal image segmentation results.

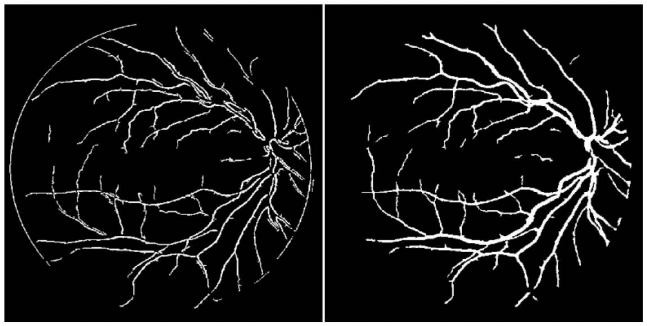

(a) Sobel operator (b) Iterative threshold method

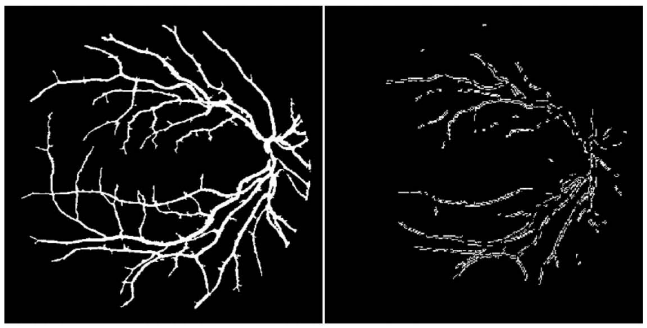

(c) Region growing method (d) Quadtree image segmentation algorithm

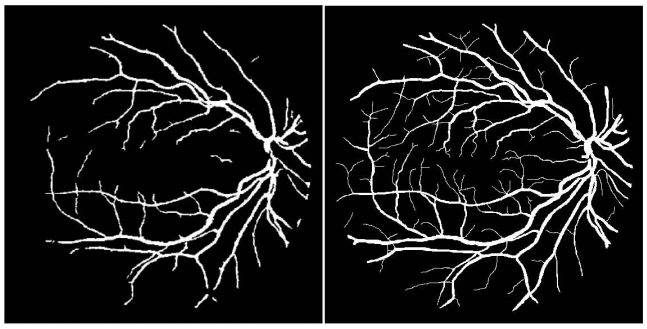

(e) Maximum variance between classes (f) Standard segmentation image

Fig. 15 Retinal image segmentation results.

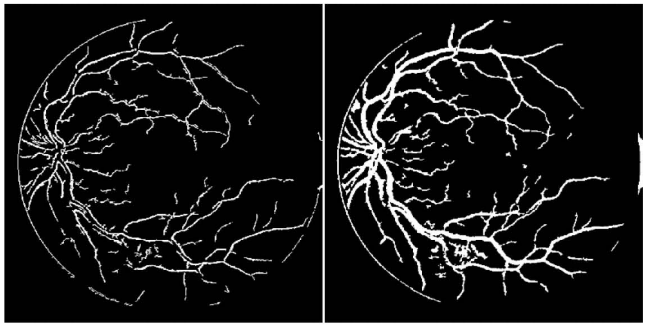

(a) Sobel operator (b) Iterative threshold method

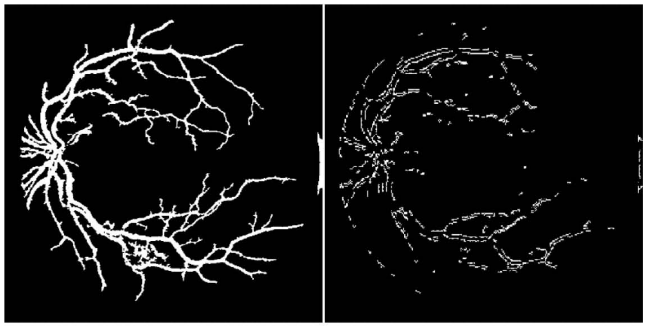

(c) Region growing method (d) Quad-tree image segmentation algorithm

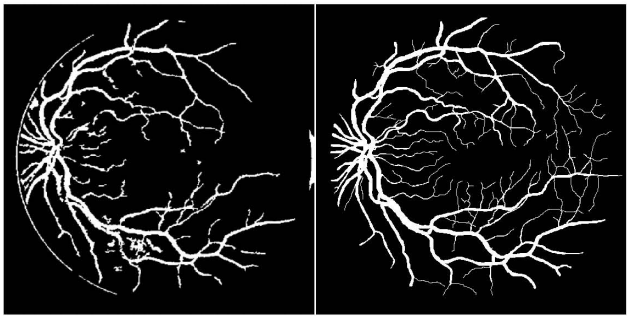

(e) Maximum variance between classes (f) Standard segmentation image

Fig. 16 Retinal image segmentation results.

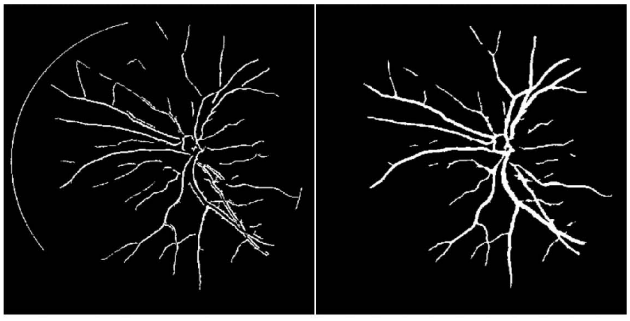

(a) Sobel operator (b) Iterative threshold method

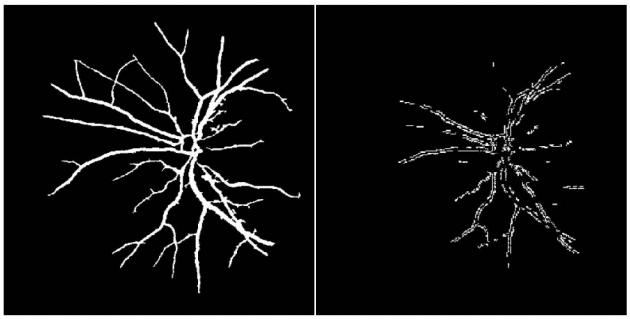

(c) Region growing method (d) Quad-tree image segmentation algorithm

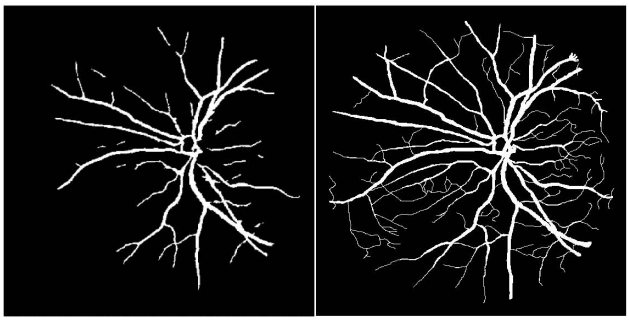

(e) Maximum variance between classes (f) Standard segmentation image

Fig. 17 Retinal image segmentation results.

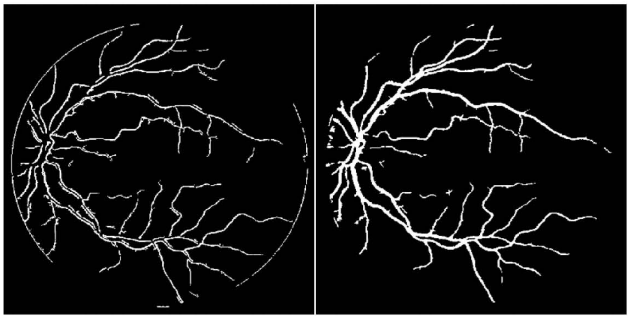

(a) Sobel operator (b) Iterative threshold method

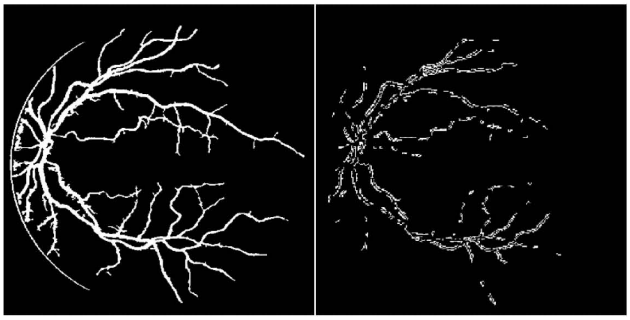

(c) Region growing method (d) Quad-tree image segmentation algorithm

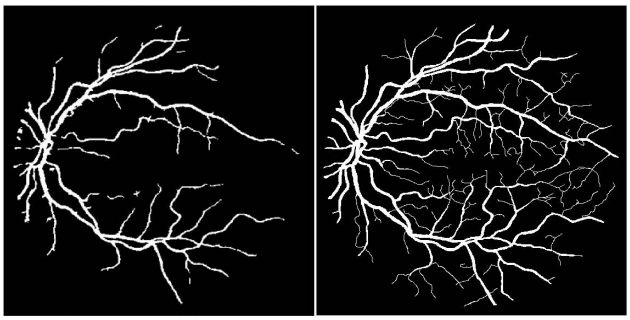

(e) Maximum variance between classes (f) Standard segmentation image

Fig. 18 Retinal image segmentation results.

TABLE 1. COMPARISON OF STANDARD IMAGE EVALUATION INDEXES BASED ON FIG. 11(A)

Performance index	Sobel operator	Iterative threshold method	Regional growth method	Quad-tree segmentation	Maximum variance between classes
Accuracy	0.9002	0.9594	0.9560	0.9092	0.9588
Sensitivity	0.2467	0.7027	0.7690	0.1522	0.6856
Fmeasure	0.3158	0.7637	0.7653	0.2383	0.7566
MCC	0.2794	0.7451	0.7410	0.2553	0.7391
precision	0.4387	0.8364	0.7616	0.5491	0.8440
Dice	0.3158	0.7637	0.7653	0.2383	0.7566
Jaccary	0.1875	0.6177	0.6198	0.1353	0.6085
Specitivity	0.9675	0.9858	0.9752	0.9871	0.9870

TABLE 2. COMPARISON OF STANDARD IMAGE EVALUATION INDEXES BASED ON FIG. 11(B)

Performance index	Sobel operator	Iterative threshold method	Regional growth method	Quad-tree segmentation	Maximum variance between classes
Accuracy	0.8994	0.9584	0.7920	0.9036	0.9575
Sensitivity	0.2851	0.6715	0.7920	0.1757	0.6569
Fmeasure	0.3755	0.7739	0.7920	0.2790	0.7666
MCC	0.3477	0.7623	0.7706	0.3120	0.7568
precision	0.5500	0.9132	0.8415	0.6773	0.9203
Dice	0.3755	0.7739	0.7920	0.2790	0.7666
Jaccary	0.2312	0.6312	0.6556	0.1621	0.6215
Specitivity	0.9723	0.9924	0.9833	0.9901	0.9932

TABLE 3. COMPARISON OF STANDARD IMAGE EVALUATION INDEXES BASED ON FIG. 11(C)

Performance index	Sobel operator	Iterative threshold method	Regional growth method	Quad-tree segmentation	Maximum variance between classes
Accuracy	0.8958	0.9440	0.9474	0.9022	0.9450
Sensitivity	0.2554	0.6958	0.7157	0.1537	0.6758
Fmeasure	0.3366	0.7201	0.7380	0.2455	0.7180
MCC	0.3045	0.6895	0.7093	0.2720	0.6893
precision	0.4935	0.7461	0.7619	0.6096	0.7657
Dice	0.3366	0.7201	0.7380	0.2455	0.7180
Jaccary	0.2023	0.5626	0.5848	0.1399	0.5600
Specitivity	0.9697	0.9726	0.9742	0.9886	0.9761

TABLE 4. COMPARISON OF STANDARD IMAGE EVALUATION INDEXES BASED ON FIG. 11(D)

Performance index	Sobel operator	Iterative threshold method	Regional growth method	Quad-tree segmentation	Maximum variance between classes
Accuracy	0.9108	0.9519	0.9561	0.9125	0.9519
Sensitivity	0.2407	0.5311	0.6172	0.1463	0.5311
Fmeasure	0.3416	0.6797	0.7298	0.2432	0.6797
MCC	0.3378	0.6878	0.7210	0.2988	0.6878
precision	0.5882	0.9440	0.8926	0.7204	0.9440
Dice	0.3416	0.6797	0.7298	0.2432	0.6797
Jaccary	0.2060	0.5149	0.5746	0.1384	0.5149
Specitivity	0.9821	0.9967	0.9921	0.9940	0.9967

TABLE 5. COMPARISON OF STANDARD IMAGE EVALUATION INDEXES BASED ON FIG. 11(E)

Performance index	Sobel operator	Iterative threshold method	Regional growth method	Quad-tree segmentation	Maximum variance between classes
Accuracy	0.9050	0.9525	0.9468	0.9116	0.9525
Sensitivity	0.2618	0.5836	0.6612	0.1869	0.5706
Fmeasure	0.3512	0.7073	0.7095	0.2935	0.7024
MCC	0.3291	0.7014	0.6827	0.3266	0.7002
precision	0.5334	0.8973	0.7655	0.6832	0.9132
Dice	0.3512	0.7073	0.7095	0.2935	0.7024
Jaccary	0.2130	0.5471	0.5498	0.1720	0.5413
Specitivity	0.9751	0.9927	0.9779	0.9906	0.9941

But it does not realize the segmentation of smaller blood vessels. Sobel operator can segment the edge zone well. The iterative threshold method enhances and further segments the main blood vessels, avoid that interference of tiny micro-vessels. The quad-tree image segmentation algorithm can segment the inflection of blood vessels very well, and the segmentation is meticulous, but it does not reflect the main blood vessels and branches.

F. Experiment and Result Analysis of Retinal Vessel Image Segmentation Based on Mathematical Morphology

In this section, the mathematical morphology algorithm was used to segment the retinal vessel images without lesions

and abnormalities shown in Fig. 11(a)-(e). The simulation results are shown in Fig. 19. It can be clearly seen that the retinal images segmented by mathematical morphology are closest to the standard images, far superior to the five image segmentation algorithms adopted above.

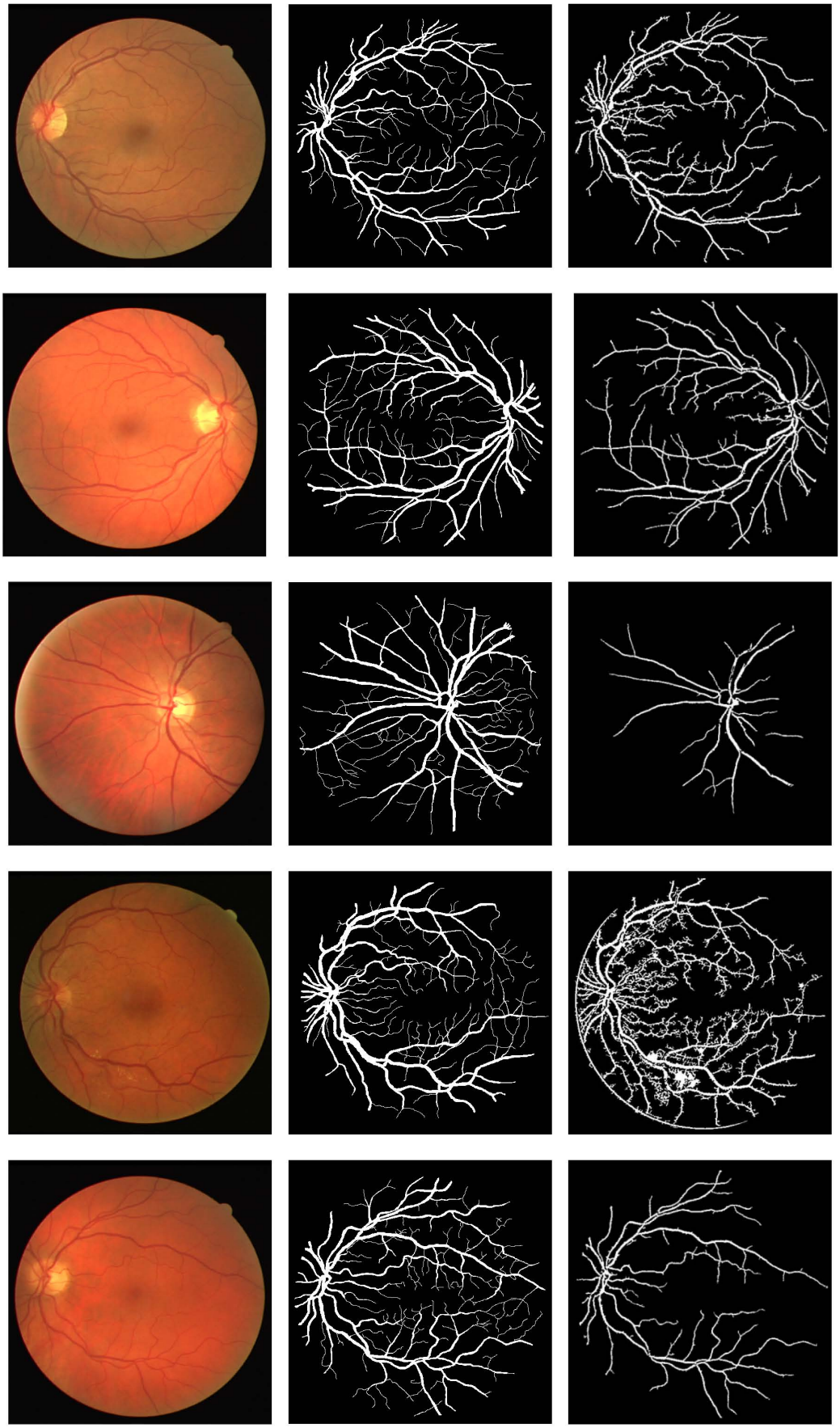

(a) Original image (b) Standard segmentation image (c) Mathematical morphology segmentation image

Fig. 19 Retinal image segmentation results based on mathematical morphology.

TABLE 6. COMPARISON OF STANDARD IMAGE EVALUATION INDEXES BASED ON MATHEMATICAL MORPHOLOGY METHOD

Performance index	Image 1	Image 2	Image 3	Image 4	Image 5
TPR	0.754211	0.648831	0.728392	0.287178	0.514946
FPR	0.0201318	0.0119357	0.0683213	0.000360473	0.0031199
ACC	0.958931	0.953325	0.911414	0.934098	0.951731
PPV	0.741847	0.723632	0.580269	0.513792	0.677479
MCC	0.76039	0.740063	0.621118	0.444983	0.666541
precision	0.783844	0.861149	0.541385	0.987762	0.944632
Dice	0.618174	0.587381	0.45045	0.28616	0.499859
Jaccary	0.979868	0.988064	0.931679	0.99964	0.99688
Specitivity	0.745211	0.648831	0.728392	0.287178	0.514946

Based on the mathematical morphology algorithm, the retinal vessel images with no lesions and abnormalities in Fig. 11(a)-(e) are segmented, and the segmentation results are compared with the standard segmentation images of retinal vessel images with no lesions and abnormalities in Fig. 12(a)-(e). Then the image segmentation performance evaluation index defined in Section 4.1 are calculated to quantitatively and qualitatively analyze the image segmentation effect. The results are listed in Table 6. By comparing the mathematical morphology algorithm with the above five image segmentation algorithms, the performance indexes such as sensitivity and accuracy of image segmentation based on mathematical morphology algorithm are better.

V. CONCLUSION

In this paper, six segmentation algorithms, including maximum variance between classes, region growing method, Sobel operator, iterative threshold method, quad-tree image segmentation and mathematical morphology algorithm, were used to segment retinal vessel images. In order to better detect the characteristics of small vessels and improve the segmentation performance, the retinal vessel images were preprocessed by using gray scale conversion, data standardization, adaptive histogram equalization, gamma correction and mathematical morphology. Simulation experiments are carried out to verify the effectiveness of the segmentation algorithms for typical images in the Drive retinal vessel image database.

REFERENCES

[1] U. Nguyen, A. Bhuiyan, L. Park, and K. Ramamohanarao, "An Effective Retinal Blood Vessel Segmentation Method Using Multi-scale Line Detection," *Pattern Recognition*, vol. 46, no. 3, pp. 703-715, 2013.

[2] L. Chen, D. Wei, and J. S. Wang, "Research on Magnetic Resonance Imaging Segmentation Algorithm," *Engineering Letters*, vol. 27, no. 3, pp. 559-567, 2019.

[3] X. D. Li, D. Wei, J. S. Wang, Q. S. Guo, and L. Chen, "Colony Image Edge Detection Algorithm Based on FCM and RBI-FCM Clustering Methods," *IAENG International Journal of Computer Science*, vol. 48, no. 2, pp. 356-363, 2021.

[4] N. R. Pal, and S. K. Pal, "A Review on Image Segmentation," *International Journal of Soft Computing & Engineering*, vol. 2, no. 1, pp. 58, 2012.

[5] M. M. Fraz, P. Remagnino, A. Remagnino, A. R. Rudnicka, C. G. Owen, P. H. Whincup and S. A. Barmana, "Quantification of Blood Vessel Calibre in Retinal Images of Multi-ethnic School Children Using a Model Based Approach," *Computerized Medical Imaging and Graphics*, vol. 37, no. 1, pp. 48-60, 2013.

[6] S. Chaudhuri, and S. Chatterjee, "Detection of Blood Vessels in Retinal Images Using Two-dimensional Matched Filters," *IEEE Transactions on Medical Imaging*, vol. 8, no. 3, pp. 263-269, 1989.

[7] C. Köse, and C. İkibaş, "Statistical Techniques for Detection of Optic Disc and Macula and Parameters Measurement in Retinal Fundus Images," *Journal of Medical & Biological Engineering*, vol. 31, no. 6, pp. 395-404, 2011.

[8] J. Widjaja, and U. Suripon, "Retinal Blood Vessel Detection Using Wavelet-matched Filter," *Optical Engineering*, vol. 52, no. 3, pp. 037204, 2013.

[9] N. P. Singh, and R. Srivastava, "Retinal Blood Vessels Segmentation by Using Gumbel Probability Distribution Function Based Matched Filter," *Computer Methods and Programs in Biomedicine*, vol. 129, pp. 40-50, 2016.

[10] Y. Yin, M. Adel, and S. Bourennane, "Retinal Vessel Segmentation Using a Probabilistic Tracking Method," *Pattern Recognition*, vol. 45, no. 4, pp. 1235-1244, 2012.

[11] I. Liu, and Y. Sun, "Recursive Tracking of Vascular Networks in Angiograms Based on the Detection-deletion Scheme," *IEEE Transactions on Medical Imaging*, vol. 12, no. 2, pp. 334-341, 1993.

[12] E. Bekkers, R. Duits, T. Berendschot, and B. Romeny, "A Multi-Orientation Analysis Approach to Retinal Vessel Tracking," *Journal of Mathematical Imaging and Vision*, vol. 49, no. 3, pp. 583-610, 2014.

[13] S. Roychowdhury, D. D. Koozekanani, and K. K. Parhi, "Blood Vessel Segmentation of Fundus Images by Major Vessel Extraction and Subimage Classification," *IEEE Journal of Biomedical & Health Informatics*, vol. 19, no. 3, pp. 1118-1128, 2015.

[14] F. Zana, and J. C. Klein, "Segmentation of Vessel-like Patterns Using Mathematical Morphology and Curvature Evaluation," *IEEE Transactions on Image Processing*, vol. 10, no. 7, pp. 1010-1019, 2001.

[15] D. Marin, A. Aquino, M. E. Gegundez-Arias, and J. M. Bravo, "A New Supervised Method for Blood Vessel Segmentation in Retinal Images by Using Gray-level and Moment Invariants-based Features," *IEEE Transactions on Medical Imaging*, vol. 30, no. 1, pp. 146-158, 2011.

[16] D. Marin, M. E. Gegundez-Arias, B. Ponte, F. Alvarez, and J. M. Bravo, "An Exudate Detection Method for Diagnosis Risk of Diabetic Macular Edema in Retinal Images Using Feature-based and Supervised Classification," *Medical and Biological Engineering and Computing*, vol. 56, no. 8, pp. 1379-1390, 2018.

[17] X. You, Q. Peng, Y. Yuan, Y. M. Cheung, and J. Lei, "Segmentation of Retinal Blood Vessels Using the Radial Projection and Semi-supervised Approach," *Pattern Recognition*, vol. 44, no. 10-11, pp. 2314-2324, 2011.

[18] G. Hassan, N. El-Bendary, A. E. Hassanien, A. Fahmy, A. M. Shoeb, and V. Snasel, "Retinal Blood Vessel Segmentation Approach Based on Mathematical Morphology," *Procedia Computer Science*, vol. 65, pp. 612-622, 2015.

[19] E. Ricci, and R. Perfetti, "Retinal Blood Vessel Segmentation Using Line Operators and Support Vector Classification," *IEEE Transactions on Medical Imaging*, vol. 26, no. 10, pp. 1357-1365, 2007.